RESEARCH ARTICLE

Bortezomib Induces Anti–Multiple Myeloma Immune Response Mediated by cGAS/STING Pathway Activation

Annamaria Gulla[1], Eugenio Morelli[1], Mehmet K. Samur[1,2,3], Cirino Botta[4], Teru Hideshima[1], Giada Bianchi[5], Mariateresa Fulciniti[1], Stefano Malvestiti[6], Rao H. Prabhala[1,7], Srikanth Talluri[1,7], Kenneth Wen[1], Yu-Tzu Tai[1], Paul G. Richardson[1], Dharminder Chauhan[1], Tomasz Sewastianik[8,9], Ruben D. Carrasco[8,10], Nikhil C. Munshi[1,7], and Kenneth C. Anderson[1]

ABSTRACT The proteasome inhibitor bortezomib induces apoptosis in multiple myeloma cells and has transformed patient outcome. Using *in vitro* as well as *in vivo* immunodeficient and immunocompetent murine multiple myeloma models, we here show that bortezomib also triggers immunogenic cell death (ICD), characterized by exposure of calreticulin on dying multiple myeloma cells, phagocytosis of tumor cells by dendritic cells, and induction of multiple myeloma–specific immunity. We identify a bortezomib-triggered specific ICD gene signature associated with better outcome in two independent cohorts of patients with multiple myeloma. Importantly, bortezomib stimulates multiple myeloma cell immunogenicity via activation of the cGAS/STING pathway and production of type I IFNs, and STING agonists significantly potentiate bortezomib-induced ICD. Our study therefore delineates mechanisms whereby bortezomib exerts immunotherapeutic activity and provides the framework for clinical trials of STING agonists with bortezomib to induce potent tumor-specific immunity and improve patient outcome in multiple myeloma.

SIGNIFICANCE: Our study demonstrates that cGAS/STING-dependent immunostimulatory activity mediates bortezomib anti-myeloma activity in experimental models and associates with clinical response to bortezomib in patients with multiple myeloma. These findings provide the rationale for clinical evaluation of STING agonists to further potentiate anti–multiple myeloma immune response.

See related commentary by Zitvogel and Kroemer, p. 405.

INTRODUCTION

Multiple myeloma is a malignancy of plasma cells in the bone marrow (BM; refs. 1, 2). Despite remarkable improvement in patient survival due to the development of proteasome inhibitors (PI) and immunomodulatory drugs (IMiD), the clinical management of patients with multiple myeloma remains challenging (1, 2). Constitutive and ongoing genetic complexity of multiple myeloma cells, coupled with the tumor-promoting, immunosuppressive BM microenvironment, underlies relapse of disease and remains an obstacle to cure (3). More recently, integration of mAbs into the treatment of both newly diagnosed and relapsed/refractory multiple myeloma has further improved patient outcome (1, 4). However, dysfunction of innate and adaptive immunity, specifically involving the T-cell compartment, highlights the need for novel approaches to enhance anti–multiple myeloma immunity and achieve more durable responses.

It is now recognized that specific antitumor immunity can be triggered by therapeutic agents via "immunogenic cell death" (ICD; refs. 5–7). During treatment-related induction of ICD, endogenous tumor cell proteins are recognized as damage-associated molecular patterns (DAMP) and activate cancer-specific immune responses (8, 9). Among several DAMPs, endoplasmic reticulum (ER) protein calreticulin (CALR) exposure on the tumor cell surface is triggered by activation of the unfolded protein response (UPR) and represents a potent "eat-me" signal, allowing for efficient phagocytosis of dying cancer cells by dendritic cells (DC) and induction of a specific antitumor immune response (10). The clinical efficacy of ICD inducers is therefore due to their ability to redirect patients' immune systems against their own tumors (9, 11). To date, identification of immunogenic properties of conventional therapeutics, such as anthracyclines and oxaliplatin, has informed their clinical application in combination with immune therapies to enhance responses in immunologically "cold" solid tumors (12, 13).

The PI bortezomib (BTZ) is one of the most effective anti–multiple myeloma agents (14, 15). Excessive protein overload in multiple myeloma cells renders them dependent on proteasome activity; conversely, PIs induce accumulation of misfolded proteins, ER stress, and multiple myeloma cell death (16). Indeed, proteasome inhibition affects the quality control of proteins critical for multiple myeloma survival (17), including those involved in DNA repair (18). Extensive preclinical studies have defined the mechanisms of action of BTZ on tumor cells and accessory cells, that is, osteoclasts, in the BM

[1]Department of Medical Oncology, Dana-Farber Cancer Institute, Harvard Medical School, Boston, Massachusetts. [2]Department of Data Sciences, Dana-Farber Cancer Institute, Boston, Massachusetts. [3]Department of Biostatistics, Harvard T.H. Chan School of Public Health, Boston, Massachusetts. [4]Department of Oncohematology, "Annunziata" Hospital, Cosenza, Italy. [5]Division of Hematology, Department of Medicine, Brigham and Women's Hospital, Harvard Medical School, Boston, Massachusetts. [6]Department of Pediatric Hematology and Oncology, Freiburg University Hospital, Freiburg, Germany. [7]VA Boston Healthcare System, Boston, Massachusetts. [8]Department of Oncologic Pathology, Dana-Farber Cancer Institute, Harvard Medical School, Boston, Massachusetts. [9]Department of Experimental Hematology, Institute of Hematology and Transfusion Medicine, Warsaw, Poland. [10]Department of Pathology, Brigham and Women's Hospital, Harvard Medical School, Boston, Massachusetts.

Note: Supplementary data for this article are available at Blood Cancer Discovery Online (https://bloodcancerdiscov.aacrjournals.org/).

Corresponding Authors: Kenneth C. Anderson, Jerome Lipper Multiple Myeloma Center, Department of Medical Oncology, Dana-Farber Cancer Institute, 450 Brookline Avenue, Boston, MA 02215. Phone: 617-632-2144; Fax: 617-632-2140; E-mail: kenneth_anderson@dfci.harvard.edu; and Annamaria Gulla. Phone: 617-632-6638; Fax: 617-632-2140; E-mail: annamaria_gulla@dfci.harvard.edu

Blood Cancer Discov 2021;2:468–83

doi: 10.1158/2643-3230.BCD-21-0047

milieu (17, 19). However, the mechanism whereby BTZ triggers ICD, as well as its biological and clinical significance, is not fully characterized (20–23). Here, we define the immunotherapeutic role of BTZ in multiple myeloma and delineate mechanisms underlying its immunostimulatory activity. We identify and validate STING signaling mediating BTZ-induced antitumor immunity, providing the preclinical rationale for clinical trials evaluating BTZ–STING agonist combination therapy to improve patient outcome in multiple myeloma.

RESULTS

BTZ Induces ICD and Stimulates Anti–Multiple Myeloma Immunity *In Vitro*

We first assessed the effect of BTZ treatment on human AMO1 and NCI-H929, as well as murine 5TGM1, multiple myeloma cell lines. BTZ induced multiple myeloma cell death in a dose-dependent manner, as measured by phosphatidylserine exposure (Fig. 1A, internal plot). As seen in Fig. 1A, BTZ also triggered a dose-dependent increase of CALR exposure on the outer leaflet of multiple myeloma cell plasma membranes and consistently activated the UPR transducer PERK pathway, evidenced by increased phosphorylation of the translation initiation factor eIF2-α (p-eIF2-α) and increased levels of CHOP and ATF4 proteins (Supplementary Fig. S1A). Confocal analysis showed that BTZ-treated multiple myeloma cells, but not untreated multiple myeloma cells, were engulfed by monocyte-derived DCs (Mo-DC) after 4 hours of coculture (Fig. 1B; Supplementary Fig. S1B); flow cytometry–based phagocytosis assay confirmed this effect in both human (AMO1 and NCI-H929) and murine 5TGM1 multiple myeloma cells (Fig. 1C; Supplementary Fig. S1C). Phagocytosis of BTZ-treated AMO1 cells stimulated maturation of DCs, as shown by increased expression of CD83 and CD86 maturation markers, which was not triggered by either untreated multiple myeloma cells or BTZ alone (Supplementary Fig. S1D). To confirm the essential role of CALR on phagocytosis by DCs, we generated murine 5TGM1 *Calr* knockout ($Calr^{KO}$) cells (Supplementary Fig. S1E). Although BTZ triggered apoptosis in both 5TGM1 wild-type (WT; $5TGM1^{WT}$) cells and the $Calr^{KO}$ clones to the same extent (Supplementary Fig. S1F), phagocytosis of BTZ-treated $Calr^{KO}$ multiple myeloma cells by DCs was inhibited (Fig. 1D). To confirm the specific on-target role of *Calr* loss in mediating suppression of phagocytosis, we stably reexpressed *Calr* in knockout cells, which efficiently restored multiple myeloma cell phagocytosis by DCs (Fig. 1E) and confirmed the obligate role of CALR exposure in this process.

Next, we assessed the stimulation of T cells by DCs loaded with BTZ-treated multiple myeloma cells. *In vitro* culture of BTZ-treated multiple myeloma cells, DCs, and T cells increased maturation and activation of both $CD4^+$ and $CD8^+$ T-cell populations (Fig. 1F; Supplementary Fig. S2A and S2B). Specifically, induction of ICD by BTZ resulted in a significant increase of $CD4^+$ effector memory (EM), total $CD8^+$, $CD8^+$ EM, and $CD8^+$ terminally differentiated EM (TEMRA) cells, which was not observed by treating DCs and T cells with BTZ in the absence of multiple myeloma cells (Supplementary Fig. S2C). Similarly, isolated T cells after cocultures showed the presence of multiple myeloma–specific cytotoxic T lymphocytes that were able to efficiently induce lysis of multiple myeloma cells (Fig. 1G). To characterize specificity of the T-cell response, we analyzed the effects of BTZ-induced cell death specifically on the naïve T-cell population in a parallel experiment. We observed increased proliferation of both $CD4^+$ and $CD8^+$ naïve T cells after coculture with BTZ-treated AMO1 or NCI-H929 cells and DCs (Supplementary Fig. S3A and S3B). Similar results were obtained using primary cells derived from patients with multiple myeloma (pdMM). We observed a dose-dependent increase in phagocytosis of BTZ-treated pdMM cells by DCs (Fig. 2A). Consistently, treatment of BM mononuclear cells (BMMC) from patients with multiple myeloma with BTZ confirmed the phenotypic changes in

Figure 1. BTZ induces ICD in multiple myeloma (MM) cells *in vitro*. **A,** Human AMO1, H929, and murine 5TGM1 multiple myeloma cell lines were treated with BTZ (1–10 nmol/L) or media (CNT) for 16 hours. CALR exposure was quantified by flow cytometry: Analysis of fluorescence intensity was assessed on viable (7-AAD–negative) cells. Floating bars show fold increase of the geometric mean normalized to CNT cells. Internal plots: percentage of apoptotic cells (Annexin-V positive) after BTZ treatment. Error bars are SD of three independent experiments for CALR analysis, and two experiments for apoptosis assays. *P* values were calculated by using two-tailed unpaired *t* test. **B** and **C,** For phagocytosis assays, Far Red–stained human AMO1, human H929, and murine 5TGM1 were left untreated or treated with BTZ for 16 hours. Then, they were cocultured with carboxyfluorescein diacetate succinimidyl ester (CFSE)–stained heterologous human DCs (hDC) or murine DCs (mDC), respectively. The JAWSII cell line was used as source of immature mDCs. Analysis was performed after 4 hours. In **B** are depicted representative confocal images showing interaction of mDCs (green) and 5TGM1 multiple myeloma cells (red), either untreated (CNT) or BTZ treated, after 4 hours of coculture. Scale bars, 20 μm. In **C** is shown the fold increase in percentage of double-positive DCs compared with CNT, as assessed by flow cytometry. Error bars are SEM of three independent experiments. Two-tailed unpaired *t* test. **D,** CFSE mDCs and 16-hour BTZ-treated or untreated Far Red-$5TGM1^{WT}$ or $Calr^{KO}$ (#1, #2, and #3) multiple myeloma cells were cocultured for 4 hours; fold increase in percentage of double-positive mDCs compared with CNT is shown. Error bars are SEM of four independent experiments. Unpaired *t* test to analyze the effect on each $Calr^{KO}$ clone compared with WT cells. **E,** Phagocytosis assay of BTZ-treated or untreated Far Red-$5TGM1^{WT}$, $Calr^{KO}$ #3, or $Calr^{KO}$ #3 re-overexpressing *Calr* (#3 *Calr* add-back) cocultured with CFSE mDCs. Fold increase of percentage of double-positive mDCs compared with CNT is shown. Error bars are SEM of three independent experiments. Unpaired two-tailed *t* test. In the right plot, Western blot of CALR protein in $5TGM1^{WT}$, $Calr^{KO}$ #3, and $Calr^{KO}$ #3-Calr add-back is shown, with GAPDH as loading control. In the add-back clones, molecular weight of full-length Calr is larger than endogenous because its cDNA is in frame with the cDNA of the 5′ end of decay accelerating factor (DAF), which encodes a signal sequence for attachment of a glycophosphatidylinositol (GPI) anchor to the C-terminus of the resulting CALR–DAF fusion protein to facilitate CALR anchoring in the plasma membrane (44). **F,** Sixteen-hour BTZ-treated or untreated AMO1 and H929 cells were cocultured for 5 days with human DCs and T cells derived from the same healthy donors. $CD4^+$ and $CD8^+$ T cells were identified based on semiunsupervised bioinformatic analysis and are represented in a uniform manifold approximation and projection (UMAP) merging independent experiments for each cell line (left plot, arrows represent differentiation pattern). On the right plots, boxplots show absolute percentage of T-cell subsets that are significantly increased in the BTZ condition (according to ANOVA pairwise comparisons): CD4_EM_CD69het ($P = 0.024$), CD8_TEMRA_CD69dim ($P = 0.029$), CD8_EM_CD69het ($P = 0.067$), and total CD8 ($P = 0.05$). Data include eight independent experiments for the AMO1 cell line and four for the H929 cell line. Defining features of T-cell subset clusters are detailed in Supplementary Fig. S2A. **G,** Sixteen-hour BTZ-treated or untreated U266 cells were cocultured with HLA-matched hDCs and T cells from the same healthy donors. After 5 days, T cells were negatively selected from both coculture conditions (CNT and BTZ) and then cultured for 24 hours with new U266 cells prestained with CFSE at 1:0, 1:1, and 1:2 target:effector (T:E) ratio, followed by 7-AAD staining and quantification of multiple myeloma cell lysis by flow cytometry. Graph shows absolute percentage of dead multiple myeloma cells. *ns*, not significant; *, $P < 0.05$; **, $P < 0.01$; ***, $P < 0.005$; ****, $P < 0.0001$.

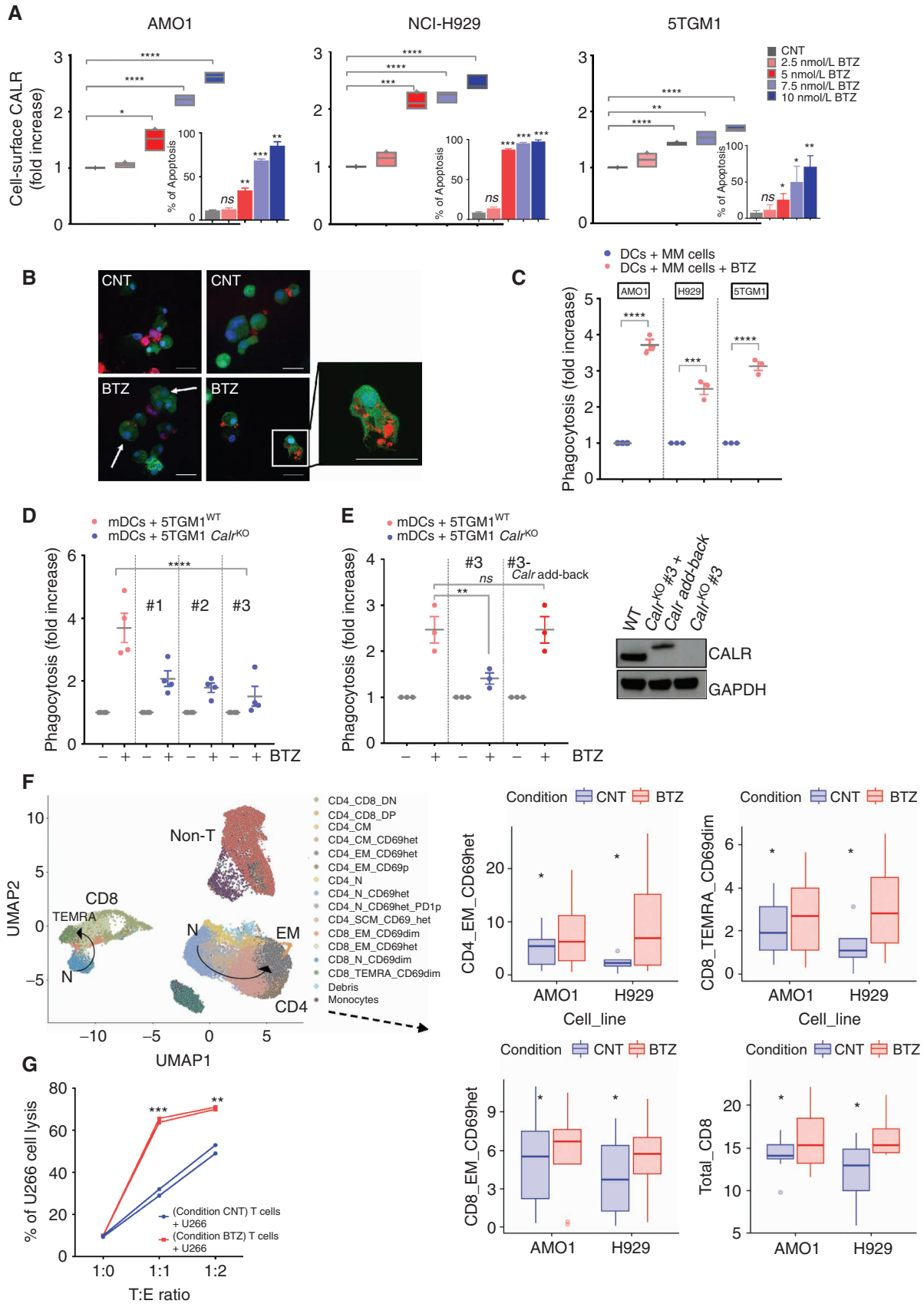
A
AMO1
NCI-H929
5TGM1
Cell-surface CALR (fold increase)
% of Apoptosis
CNT
2.5 nmol/L BTZ
5 nmol/L BTZ
7.5 nmol/L BTZ
10 nmol/L BTZ
B
CNT
BTZ
C
DCs + MM cells
DCs + MM cells + BTZ
Phagocytosis (fold increase)
D
mDCs + 5TGM1WT
mDCs + 5TGM1 CalrKO
#1
#2
#3
BTZ
E
#3-Calr add-back
WT
Calr-KO#3 + Calr add-back
Calr-KO#3
CALR
GAPDH
F
UMAP1
UMAP2
Non-T
CD8 TEMRA
N
EM
CD4
CD4_CD8_DN
CD4_CD8_DP
CD4_CM
CD4_CM_CD69het
CD4_EM_CD69het
CD4_EM_CD69p
CD4_N
CD4_N_CD69het
CD4_N_CD69het_PD1p
CD4_SCM_CD69_het
CD8_EM_CD69dim
CD8_EM_CD69het
CD8_N_CD69dim
CD8_TEMRA_CD69dim
Debris
Monocytes
Condition CNT BTZ
CD4_EM_CD69het
CD8_TEMRA_CD69dim
Cell_line
AMO1
H929
CD8_EM_CD69het
Total_CD8
G
% of U266 cell lysis
(Condition CNT) T cells + U266
(Condition BTZ) T cells + U266
T:E ratio

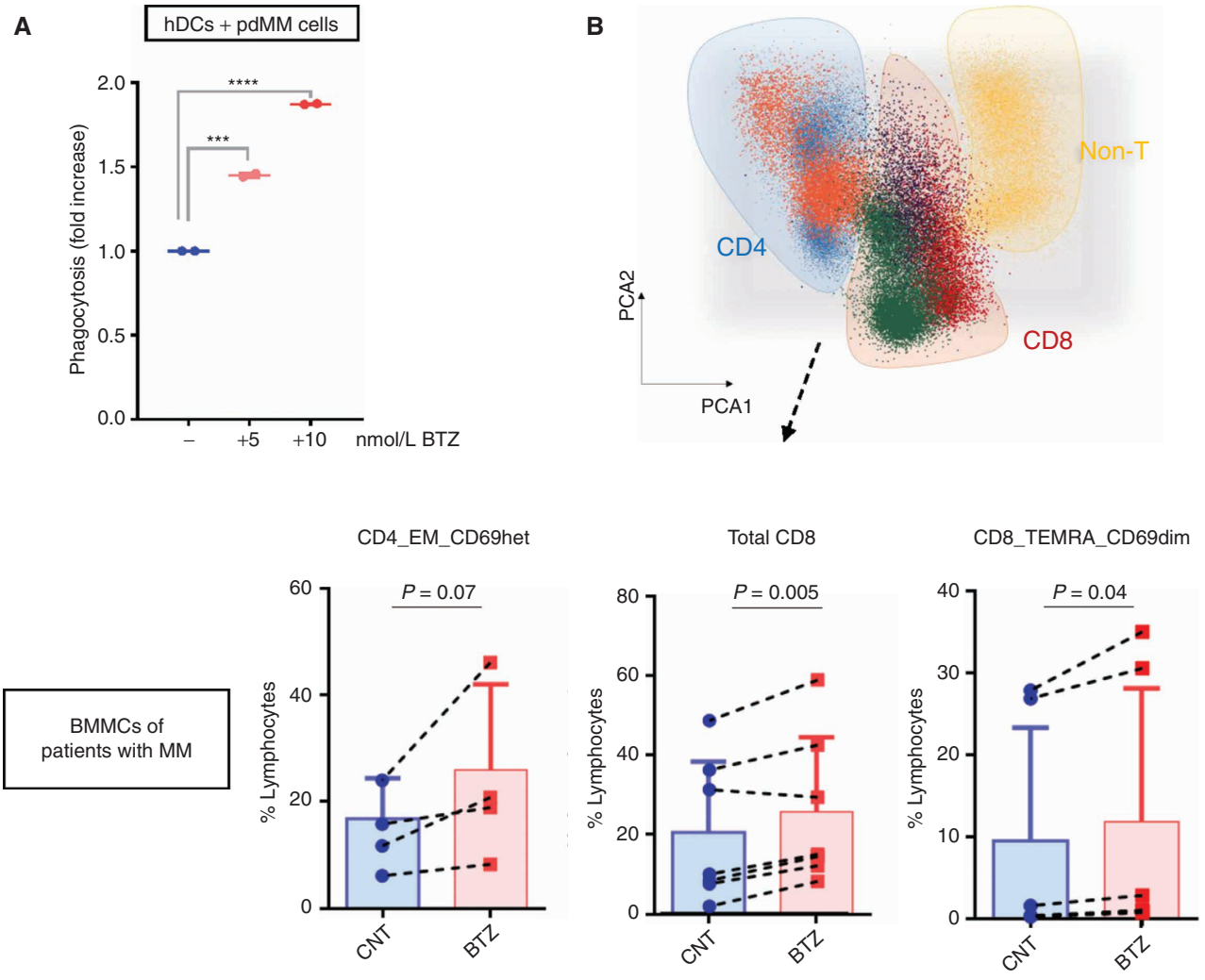

Figure 2. BTZ-mediated induction of immune response in patient-derived multiple myeloma (MM) cells *in vitro*. **A,** Flow cytometry–based phagocytosis assay: CFSE human DCs (hDC) from healthy donors were cocultured for 4 hours with BTZ-treated (5 and 10 nmol/L) or untreated Far Red pdMMs. Shown is the fold increase in percentage of double-positive DCs compared with CNT. Error bars are SEM of two independent experiments. ***, $P < 0.001$; ****, $P < 0.0001$ compared with CNT; two-tailed unpaired *t* test. **B,** Total autologous BMMCs from patients with multiple myeloma were cultured in the presence or absence of BTZ (5 nmol/L). After 5 days, flow cytometry analysis on $CD4^+$ ($n = 4$) and $CD8^+$ ($n = 6$) T cells was performed. Top plot, automatic population separator showing cells clustered based on their immunophenotypes. Bottom plots, boxplots show absolute percentage of T-cell subsets that are significantly increased in the BTZ condition (according to paired Student *t* test): CD4_EM_CD69het ($P = 0.07$), CD8_TEMRA_CD69dim ($P = 0.04$), and total CD8 ($P = 0.005$).

both $CD4^+$ and $CD8^+$ T-cell populations (Fig. 2B). Altogether, these data show that BTZ increases the immunogenicity of multiple myeloma cells, thereby stimulating an anti–multiple myeloma immune response *in vitro*.

BTZ Stimulates Anti–Multiple Myeloma Immunity *In Vivo* via Induction of ICD

To test the relevance of ICD in BTZ-induced anti–multiple myeloma activity *in vivo*, we used the syngeneic immunocompetent 5T murine model of multiple myeloma (24). We found that low doses of BTZ (0.5 mg/kg twice/week for 2 weeks) inhibited growth of $5TGM1^{WT}$ cells engrafted in immunocompetent (C57BL/KaLwRij) mice (Fig. 3A) to a greater extent than when these cells were engrafted in immunodeficient hosts (SCID/NOD; Fig. 3B). Importantly, this effect was directly linked to ICD induction, because it was abrogated in immunocompetent mice bearing 5TGM1 $Calr^{KO}$ tumors (Fig. 3C) in which the delay of tumor growth was similar to that observed in the immunodeficient hosts (Fig. 3D). Taken together, these results suggest that the effects of BTZ are mediated, at least in part, by the immune system.

We next tested whether, after the regression of tumor growth, the mice were further protected against a tumor rechallenge. Injection of live $5TGM1^{WT}$ cells 2 weeks after BTZ-induced tumor regression did not result in tumor development, and 100% of mice were alive at the end of observation (day 30 after rechallenge; Fig. 3E). *Ex vivo* enzyme-linked immunospot (ELISPOT), using splenocytes harvested from mice treated under the same conditions, confirmed the generation

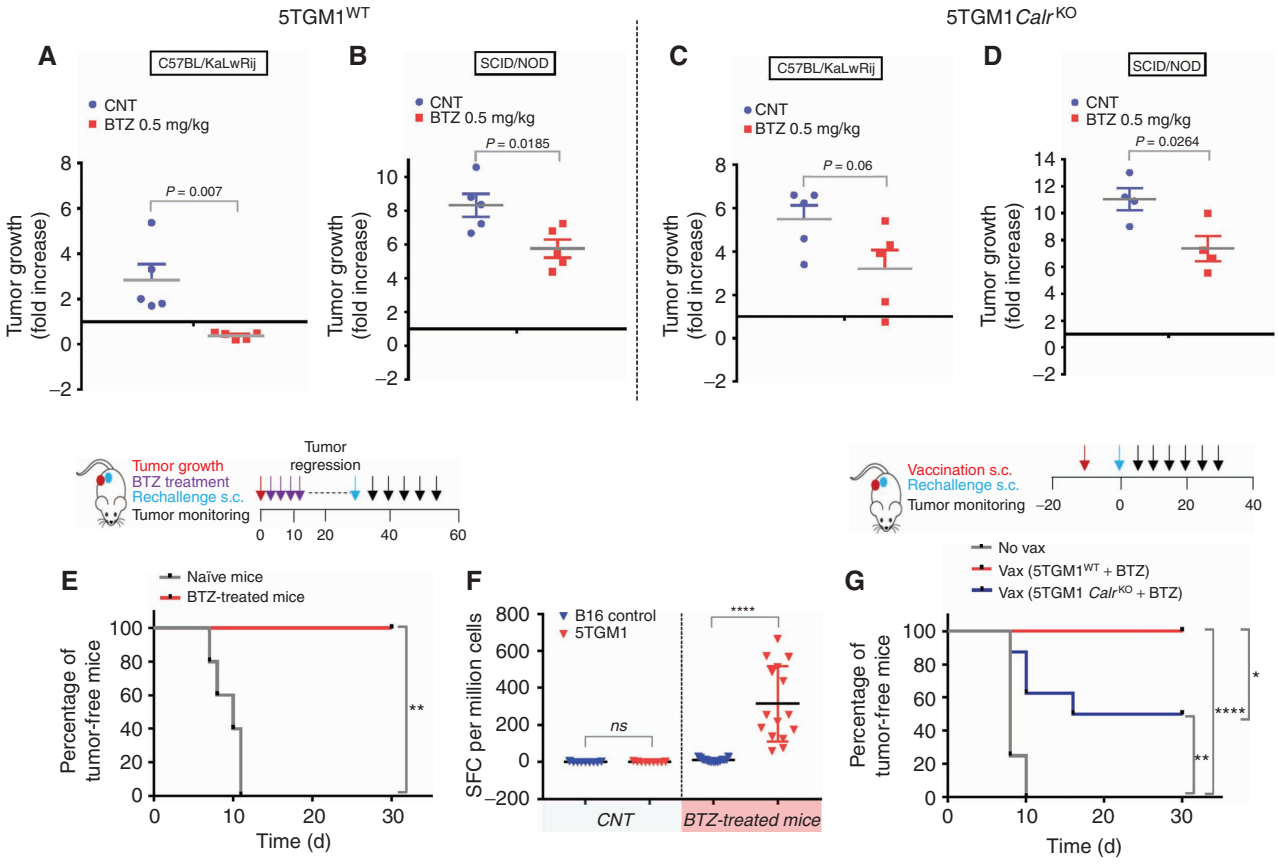

Figure 3. BTZ induces ICD in a syngeneic murine model of multiple myeloma (MM). **A–D,** *In vivo* growth of subcutaneous xenografts of 5TGM1^{WT} (**A** and **B**) or 5TGM1 *Calr*^{KO} (**C** and **D**) multiple myeloma cells in immunocompetent C57BL/KaLwRij (**A** and **C**) or immunodeficient SCID/NOD (**B** and **D**) mice treated with either PBS (CNT) or BTZ (0.5 mg/kg twice/week for 2 weeks) when tumors became measurable by electronic caliper. Fold increase of tumor growth from day 1 (start of treatment) to day 8 ± SD ($n = 5$ animals per group in **A**, **B**, and **C** and $n = 4$ in **D**). One representative experiment of two yielding similar results is shown for each condition. *P* values were calculated using unpaired Student *t* test. **E,** Immunocompetent C57BL/KaLwRij ($n = 5$) bearing 5TGM1^{WT} tumors were treated with BTZ as in **A**. Two weeks after tumor regression, BTZ-treated mice ($n = 5$) were rechallenged with viable 5TGM1 cells, along with naïve mice ($n = 5$), and percentage of mice remaining tumor free in the two cohorts is shown according to the Kaplan–Meier method. *P* value was calculated by using the log-rank test. Schema of the experimental design is shown in top plot. **F,** *Ex vivo* ELISPOT was performed on splenocytes harvested from mice treated as in **E**. Splenocytes were left unstimulated or stimulated with B16 tumor cells as negative control and 5TGM1 or anti-CD3 as positive control to test T-cell avidity in an IFNγ ELISPOT assay. Spot-forming colonies (SFC) per million are represented for $n = 3$ naïve and $n = 5$ BTZ-treated mice ± SD. ELISPOT experiments were performed in triplicate wells per sample; unpaired Student *t* test for statistical analysis. ELISPOT images are shown as Supplementary Fig. S4A. **G,** *In vitro* BTZ-treated 5TGM1^{WT} or *Calr*^{KO} cells were injected into naïve mice; control mice (No vax) received PBS as a negative control. Mice ($n = 8$ animals per group) were rechallenged with viable 5TGM1 cells 1 week later, and percentage of mice remaining tumor free in the three cohorts is shown according to the Kaplan–Meier method. The log-rank test was used for statistical significance. Schema of the experimental design is shown in top plot. *ns*, not significant; *, $P < 0.05$; **, $P < 0.01$; ****, $P < 0.0001$.

of a robust immune response against multiple myeloma cells that could protect against rechallenge (Fig. 3F; Supplementary Fig. S4A). In a similar attempt to prove the induction of immunologic memory after BTZ-induced cell death, we also assessed whether vaccination of C57BL/KaLwRij mice with *in vitro* BTZ-treated 5TGM1 cells could protect mice against challenge with viable 5TGM1 cells. Nonvaccinated mice developed palpable tumors 1 week after 5TGM1 injection, whereas no tumor developed in vaccinated mice even after 30 days (Fig. 3G). Mice were next similarly vaccinated with BTZ-treated 5TGM1 *Calr*^{KO} cells and challenged 1 week later with injection of live WT 5TGM1 cells. Only 50% of vaccinated mice were tumor free at day 30 (Fig. 3G). Altogether, these data indicate that induction of ICD by BTZ induces a protective antitumor response *in vivo*.

An ICD-Related Signature Predicts Clinical Outcome in Patients with Multiple Myeloma after BTZ Treatment

To confirm the biological sequelae of ICD induction by BTZ in tumors *in vivo*, we performed RNA sequencing (RNA-seq) analysis of 5GTM1 WT and 5GTM1 *Calr*^{KO} tumors grown in C57BL/KaLwRij immunocompetent mice. The transcriptional changes induced by BTZ in 5GTM1 WT tumors were consistent with activation of an immune response (i.e., inflammatory response and regulation of immune system process), whereas loss of *Calr* in 5GTM1 tumors decreased this effect and revealed instead an enrichment in signaling related to direct BTZ cytotoxicity (i.e., regulation of protein polyubiquitination and positive regulation

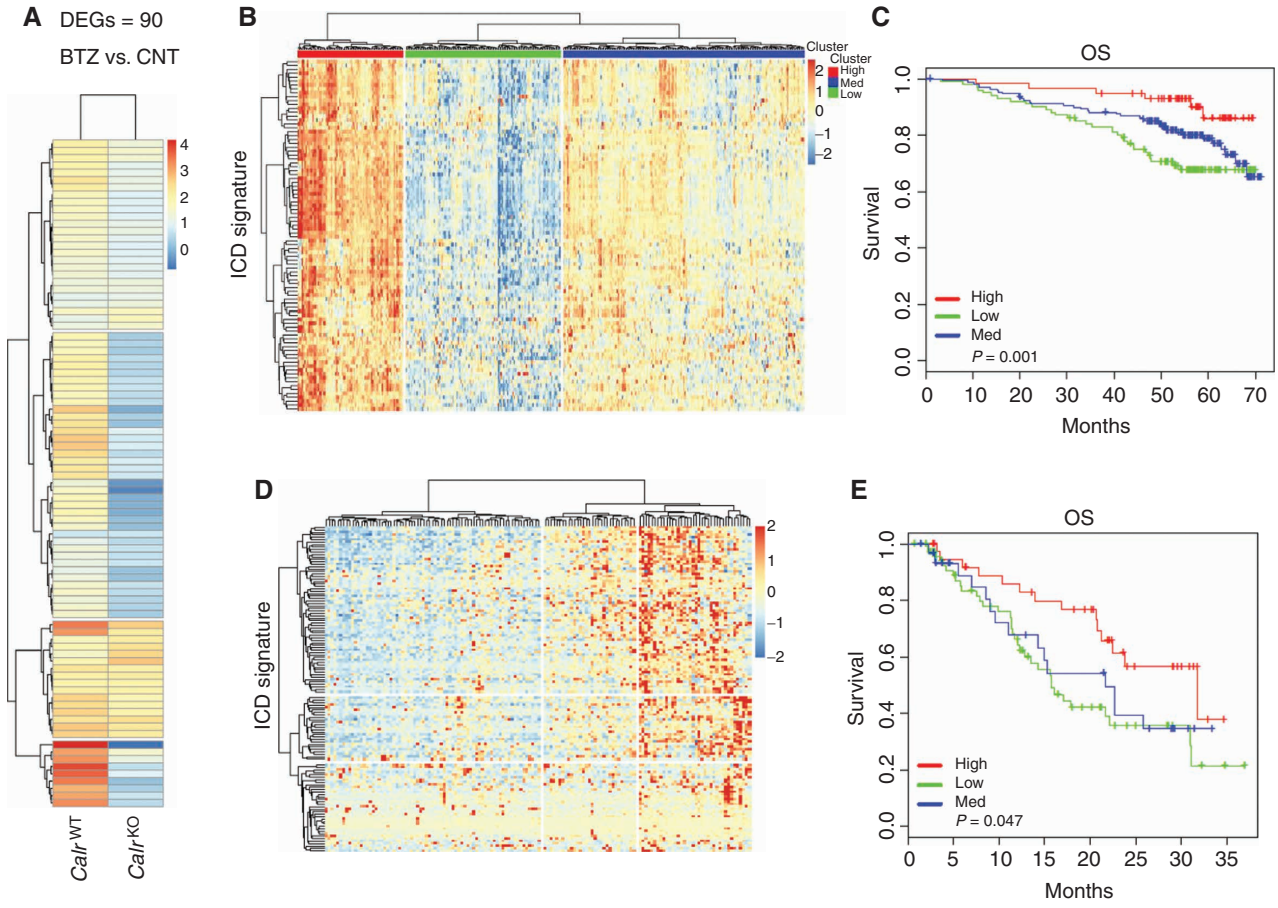

Figure 4. An ICD-related signature predicts clinical outcome in patients with multiple myeloma (MM) after BTZ treatment. **A,** Log_2 fold-change (log2FC) values for 90 genes, as determined by RNA-seq analysis, in 5TGM1^{WT} or 5TGM1 *Calr*^{KO} tumors growing in immunocompetent C57BL/KaLwRij mice after two BTZ treatments (0.5 mg/kg). Columns represent the conditions, and rows are those differentially expressed genes (DEG) in the BTZ-treated cohort compared with the CNT cohort ($n = 3$ mice per group). FC > 1.5 and FDR < 0.05. **B** and **D,** Analysis of the human orthologs of this 90-gene murine ICD signature was performed in CD138$^+$ multiple myeloma cells from two independent BTZ-treated cohorts of patients with multiple myeloma: IFM/DFCI 2009 dataset ($n = 327$; **B**) and GSE9782 ($n = 152$; **D**). Heatmaps identified three clusters of patients with multiple myeloma showing high (red), medium (blue), and low (green) expression of these signature genes. **C** and **E,** Kaplan–Meier plots show OS for the three patient clusters identified by expression of the 90 ICD gene signature. Red, blue, and green curves represent OS of patients with high, medium, and low ICD signature expression, respectively. Log-rank test *P* values for IFM/DCFI 2009 dataset and GSE9782 dataset are 0.01 and 0.047.

of autophagy; Supplementary Fig. S5A). Focused analysis of the most upregulated genes after BTZ treatment in mice bearing 5GTM1 WT tumors identified a set of 90 immune-related genes composing an ICD signature, which was not similarly modulated in 5GTM1 *Calr*^{KO} tumors (Fig. 4A; Supplementary Table S1). Importantly, we found that high expression of the human orthologs of the murine ICD gene signature was strongly positively correlated with clinical outcome of patients with multiple myeloma uniformly treated with BTZ-based regimens in the IFM/DFCI clinical study [IFM/DFCI 2009; ref. 25; overall survival (OS) *P* value = 0.01; Fig. 4B and C]. The predictive value of the identified ICD signature was also confirmed in an independent dataset (GSE9782; ref. 26; OS *P* value = 0.047) in which patients received only BTZ as frontline therapy (Fig. 4D and E). To gain further insight into the biological significance of the genes included in the ICD signature, we performed gene ontology analysis showing enrichment in the following pathways: inflammatory response, regulation of immune effector process, cellular response to cytokine stimulus, cell adhesion, cargo activity receptor, cytokine production, and positive regulation of immune response. Interestingly, 57 of 90 genes were identified as IFN-stimulated genes (ISG) using the Interferome database (ref. 27; Supplementary Fig. S6A). These data suggest that induction of ICD by BTZ treatment contributes to a clinical benefit in patients with multiple myeloma and that an inflammatory response involving ISGs may be an important mediator of this outcome.

BTZ Activates a "Viral Mimicry" State in Multiple Myeloma Cells, Which Is Required for Its Activity *In Vivo*

Transcriptional activation of ISGs by inducers of ICD is consistent with a "viral mimicry" state (28, 29). Specifically, type I IFN response and inflammatory chemokines (such as CXCL9) create an inflammatory microenvironment and are required for optimal therapeutic efficacy of agents inducing ICD (28–30). We therefore next examined induction of a type I

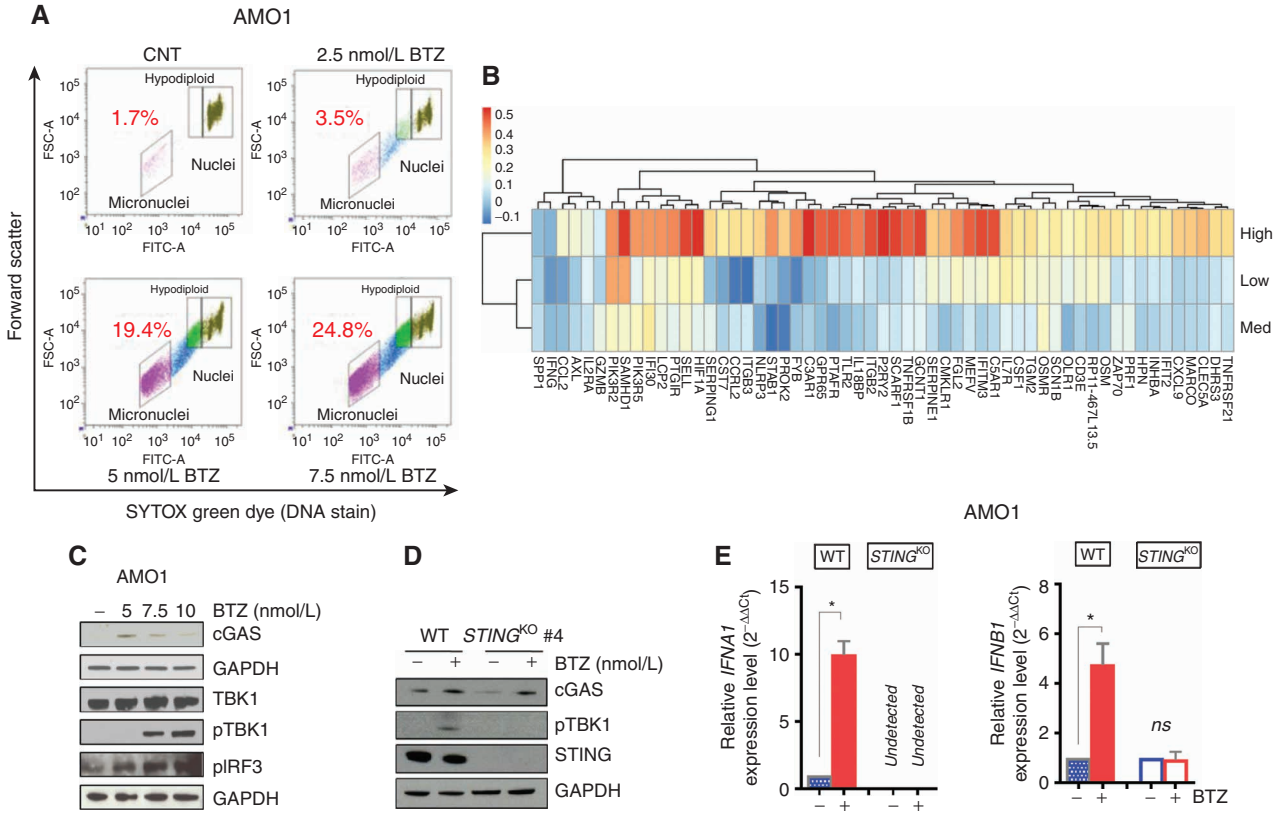

Figure 5. BTZ induces IFNI signaling and promotes T-cell activation via the cGAS/STING pathway. **A,** AMO1 cells were treated with BTZ (0 to 7.5 nmol/L) for 16 hours. Viable cells were separated using Ficoll gradient centrifugation. Dot plots show micronuclei quantification as a percentage of diploid nuclei, as detected by flow cytometry. In the analysis, remaining apoptotic cells were gated out using ethidium monoazide dye that crosses the compromised outer membrane of apoptotic and necrotic cells. One of two experiments yielding similar results is shown. **B,** Heatmap shows the correlation analysis of 57 ISGs included in the ICD signature with STING/TMEM173 gene expression across the three subsets of patients with multiple myeloma (IFM/DFCI 2009 dataset) expressing high, medium, and low levels of the ICD signature (as in Fig. 4). Blue and red identify lower and higher correlation scores, respectively. **C,** Western blot (WB) analysis of the STING pathway in AMO1 cells treated with increasing doses of BTZ (5–10 nmol/L) for 16 hours. GAPDH was used as loading control to quantify cGAS, TBK1, phosphor-TBK1 (pTBK1), and pIRF3 expression. **D,** WB analysis of cGAS, pTBK1, and STING in AMO^{WT} and *STING*^{KO} cells treated with BTZ (5 nmol/L). **E,** qRT-PCR analysis of IFNA1 and IFNB1 mRNAs in AMO^{WT} and *STING*^{KO} cells either untreated or after BTZ (5 nmol/L). Raw cross threshold (Ct) values were normalized to GAPDH housekeeping gene and expressed as ΔΔCt values. Data are the average of three independent experiments performed in triplicate. *ns*, not significant; *, $P < 0.05$; unpaired *t* test. (*continued on next page*)

IFN response by treating AMO1 and NCI-H929 multiple myeloma cells with BTZ *in vitro*. RNA-seq analysis of AMO1 cells treated with BTZ confirmed positive enrichment of gene sets included in the type I IFN response hallmark signature (Supplementary Fig. S7A), which was also validated by qRT-PCR showing increased *IFNA1*, *IFNB1*, and *CXCL9* transcripts in AMO1 and NCI-H929 multiple myeloma cells after BTZ treatment (Supplementary Fig. S7B). We next assessed the contribution of this type I IFN response to the anti–multiple myeloma activity of BTZ *in vivo*. Neutralization of type I IFN signaling in both multiple myeloma and host cells, using the type I IFN receptor 1 (IFNAR1)–specific MAR1-5A3 mAb, significantly decreased the efficacy of BTZ against 5TGM1 tumors as compared with isotype control mAb (Supplementary Fig. S7C). qRT-PCR analysis on harvested tumors confirmed that the MAR1-5A3 mAb blocked *Cxcl9* transcript accumulation in tumors from BTZ-treated mice (Supplementary Fig. S7D). In a parallel analysis of patients with multiple myeloma uniformly treated with BTZ-containing regimens (IFM/DFCI 2009), we found that low expression of *CXCL9* transcript in CD138$^+$ multiple myeloma cells independently correlates with poor clinical outcome (OS P value = 0.037; Supplementary Fig. S7E). These studies indicate that BTZ induces a viral mimicry state in multiple myeloma cells and that this type I IFN response is required for optimal *in vivo* response.

BTZ Induces Type I IFN Signaling via Activation of the cGAS/STING Pathway

BTZ induces genomic instability and inhibits DNA repair in multiple myeloma cells (18). Recent studies show that damaged DNA can be detected outside the nucleus and induce an immunostimulatory response, mimicking a viral attack and activating a type I IFN response (31, 32). We next showed that BTZ induced a dose-dependent increase of DNA content in the cytoplasm of AMO1 and NCI-H929 multiple myeloma cells, detected in the form of micronuclei by flow cytometry (Fig. 5A; Supplementary Fig. S8A and S8B). Previous studies demonstrated that cGAS can directly sense micronuclei formation and link genomic instability to innate immunity by directly activating the STING/TMEM173 pathway (32–34).

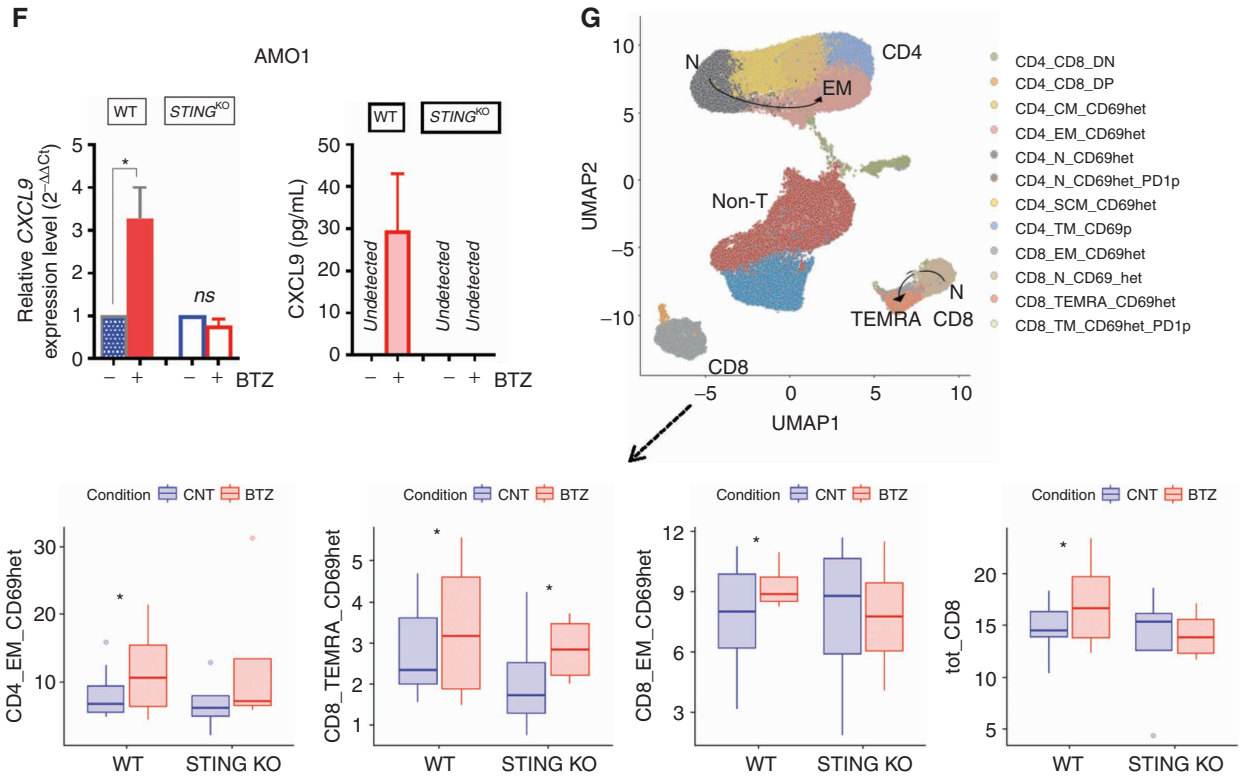

Figure 5. ***(Continued)*** **F,** Analysis of modulation of CXCL9 in AMO^{WT} and *STING*^{KO} cells after treatment with BTZ (5 nmol/L) for 16 hours by qRT-PCR analysis of CXCL9 mRNA (left) and ELISA quantification of extracellular CXCL9 (right). Data are means of two independent experiments ± SEM. *, $P < 0.1$ (unpaired Student *t* test) compared with untreated cells. **G,** BTZ-treated or untreated AMO^{WT} and *STING*^{KO} cells were cocultured with human DCs and T cells from the same healthy donors for 5 days. Cells were analyzed using a bioinformatic pipeline, and results reported in a uniform manifold approximation and projection (UMAP) including $n = 8$ independent experiments for the AMO1^{WT} cell line and $n = 4$ for the AMO1 *STING*^{KO} cell line (top). Bottom plots show absolute percentage of T-cell subsets and increase in BTZ-treated compared with CNT in both cell lines: CD4_EM_CD69het (AMO^{WT}: $P = 0.027$; *STING*^{KO}: $P =$ ns), CD8_TEMRA_CD69het (AMO^{WT}: $P = 0.1$; *STING*^{KO}: $P = 0.09$), CD8_EM_CD69het (AMO^{WT}: $P = 0.064$; *STING*^{KO}: $P =$ ns), and total CD8 (AMO^{WT}: $P = 0.09$; *STING*^{KO}: $P =$ ns); *, $P < 0.1$; ANOVA pairwise. Defining features of T-cell subset clusters are detailed in Supplementary Fig. S8H.

Importantly, we found that expression of the ISGs included in the ICD signature was positively correlated with STING expression in the cluster of patients with high levels of ICD signature genes (Fig. 5B). Moreover, we also found that BTZ treatment of both AMO1 and NCI-H929 multiple myeloma cells induces accumulation of the cytosolic DNA sensor cGAS, which activates the adaptor molecule STING and in turn leads to phosphorylation by TBK1 kinase of IRF3, a well-known transcription factor of type I IFN genes (ref. 35; Fig. 5C; Supplementary Fig. S8C). We therefore hypothesized that BTZ may induce type I IFN signaling via activation of the cGAS/STING pathway. To test this possibility, we generated human AMO1 *STING*^{KO} and murine 5TGM1 *STING*^{KO} multiple myeloma cell lines (Supplementary Fig. S8D) and confirmed that KO of STING did not alter CALR exposure process after treatment with BTZ in both edited cell lines (Supplementary Fig. S8E). Although BTZ treatment significantly increased accumulation of cGAS, KO of *STING* blocked activation of downstream signaling, including p-TBK1 in AMO1 cells (Fig. 5D). The impairment of STING pathway activation was consistent with abrogation of a type I IFN response after BTZ treatment, and RNA-seq analysis showed that BTZ treatment in AMO1 multiple myeloma cells lacking *STING* did not activate transcription of genes in the IFN response or increase the levels of *IFNA1* and *IFNB1* transcripts, as detected by qRT-PCR (Fig. 5E; Supplementary Fig. S8F). Likewise, abrogation of IFN response after BTZ treatment was also confirmed in 5TGM1 *STING*^{KO} cells (Supplementary Fig. S8G). Moreover, neither the *CXCL9* transcript nor its secreted form was detected after treatment of AMO1 *STING*^{KO} clones with BTZ (Fig. 5E and F). This block of type I IFN response in multiple myeloma cells resulted in impaired T-cell response: No significant increase of CD4$^+$ EM, total CD8$^+$, and CD8$^+$ EM cells was noted after coculture of DCs with BTZ-treated AMO1 *STING*^{KO} cells as compared with BTZ-treated AMO1 WT clones (Fig. 5G; Supplementary Fig. S8H). These findings indicate that type I IFN response in multiple myeloma cells triggered by BTZ is mediated by the cGAS/STING pathway and enhances anti–multiple myeloma T-cell responses.

STING Agonists Potentiate BTZ-Induced Antitumor Immunity

Pharmacologic activation of the STING pathway represents a promising strategy to overcome immunosuppression in the tumor microenvironment (36–38). We found that the synthetic cyclic dinucleotide STING agonist ADU-S100 (38, 39) can significantly increase the activation of STING signaling after BTZ treatment *in vitro*, as evidenced by higher

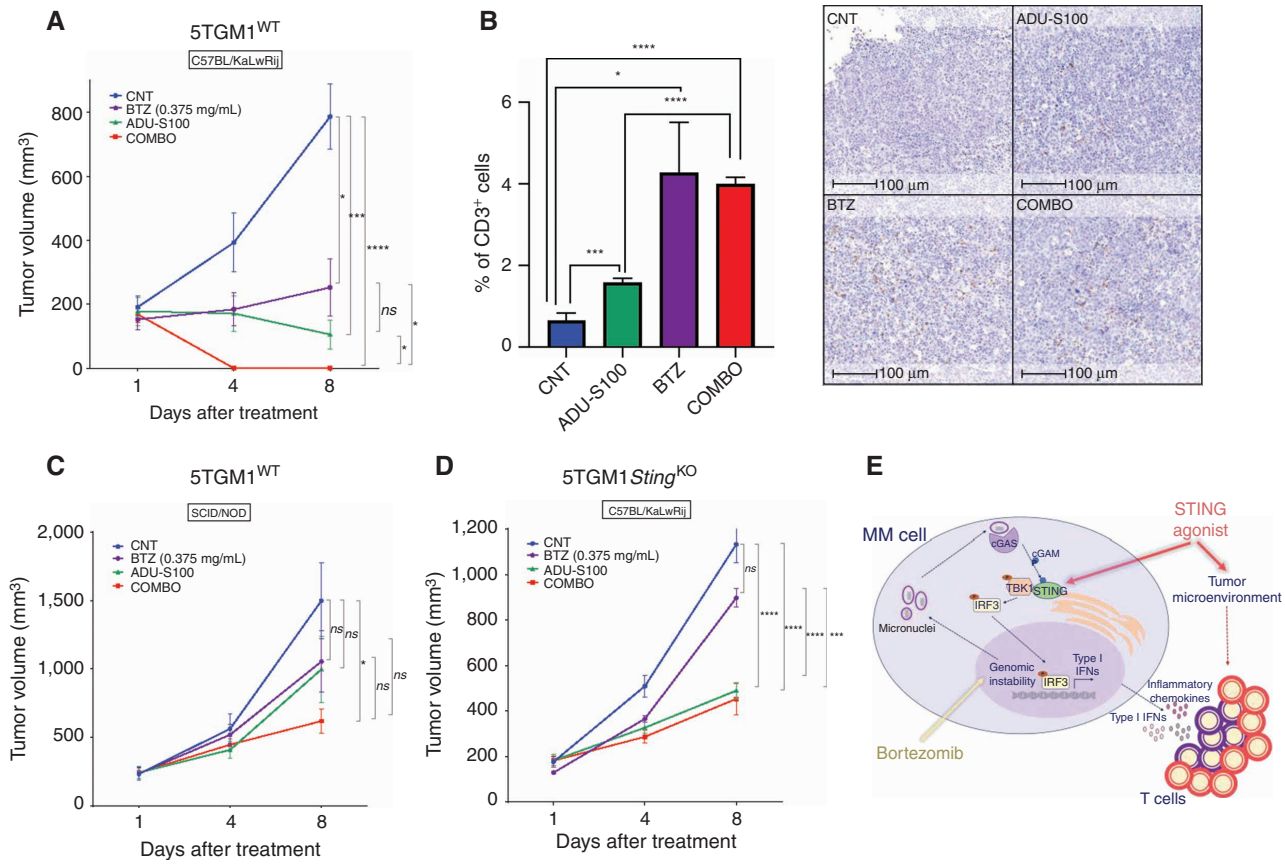

Figure 6. STING agonists potentiate BTZ-induced antitumor immunity. **A,** Tumor volume changes of subcutaneous 5TGM1^{WT} xenografts in C57BL/KaLwRij mice treated with PBS (CNT), BTZ (0.375 mg/kg twice/week for 2 weeks), intratumoral administration of ADU-S100 (100 µg, days 1 and 2), or the combination of BTZ and ADU-S100. Average tumor growth ± SEM for each group ($n = 5$) is reported. *P* values were calculated using unpaired Student *t* test. **B,** Percentage of positive cells for CD3 staining. Graph depicts the mean ± SD of tumor xenograft sections 100 µm apart from representative CNT-, BTZ-, ADU-S100–, and COMBO-treated mice. Welch *t* test was used for statistical analysis. On the right, representative images of IHC CD3 staining on tumors retrieved from each group. Scale bars, 100 µm. **C,** Tumor volume changes of subcutaneous 5TGM1^{WT} xenografts in SCID/NOD mice treated as in **A**. Average tumor growth ± SEM for each group ($n = 6$) is reported. Unpaired Student *t* test. **D,** Tumor volume analysis of subcutaneous 5TGM1 *STING*^{KO} xenografts in C57BL/KaLwRij mice treated as in **A**. Average tumor growth ± SEM for each group ($n = 5$) is reported. Unpaired Student *t* test. **E,** Schematic model. Combination of BTZ [which augments anti–multiple myeloma (MM) immune response by stimulating the STING pathway by increasing genomic instability] and STING agonist (which activates intratumor and tumor microenvironment STING downstream signaling) potentiates type I IFN response and increases T-cell recruitment and activation. *ns*, not significant; *, $P < 0.05$; ***, $P < 0.005$; ****, $P < 0.001$.

levels of phosphorylated TBK1 kinase (Supplementary Fig. S9A) and increased transcription of *IFNA1* and *IFNB1* (Supplementary Fig. S9B). Thus, we tested whether combining BTZ and ADU-S100 could increase the tumor T-cell infiltration and enhance the antitumor activity *in vivo*. C57BL/KaLwRij immunocompetent mice bearing 5TGM1 tumors were randomized to receive (i) BTZ alone (0.375 mg/kg twice/week for 2 weeks), (ii) peritumoral administration of ADU-S100 (100 µg on days 1 and 2), (iii) both drugs, or (iv) PBS as control. Mice treated with the combination showed the most significant reduction of tumor growth, with a complete regression of the tumors (COMBO vs. BTZ $P = 0.029$; COMBO vs. ADU-S100 $P = 0.05$; Fig. 6A). IHC analysis of tumors retrieved after one administration of the drugs showed that treatment with either BTZ or ADU-S100 alone or in combination increased CD3$^+$ T-cell infiltration within tumors (Fig. 6B). Murine 5TGM1 cells are sensitive to direct killing by ADU-S100 treatment *in vitro* (Supplementary Fig. S9C). Thus, we next performed an identical *in vivo* study in immunodeficient NOD/SCID mice to examine whether ADU-S100 antagonizes multiple myeloma growth *in vivo* via an immunomodulatory activity or via a direct cytotoxicity. As shown in Fig. 6C, the absence of the immune system abrogated the antitumor effects of both BTZ and ADU-S100 (100 µg on days 1 and 2), indicating that the observed tumor regression in the presence of the immune system was primarily due to an antitumor immune response. To further confirm the role of the intrinsic stimulation of intratumoral STING in mediating immune activation, we also tested the effect of BTZ–STING agonist combination in immunocompetent mice bearing *STING*^{KO} tumors. Antitumor activity of BTZ was significantly abrogated against tumors lacking *STING* (Fig. 6D), whereas ADU-S100 still retained a partial anti–multiple myeloma activity most likely due to stimulation of the STING pathway in the immune microenvironment cells (37, 38). Taken together, these results indicate a central role for STING in mediating the anti–multiple myeloma immune response induced by BTZ and show that STING agonist

augments this effect by further promoting an immunogenic microenvironment (Fig. 6E).

DISCUSSION

Immune dysfunction poses a challenge to effective anti–multiple myeloma therapy and complete elimination of minimal residual disease (3). Although the mechanisms of action of anti–multiple myeloma agents have been characterized, their *in vivo* effects on the dynamic interplay between tumor cells and the immune system are yet to be defined (3) and may inform optimal combination treatment approaches in patients. In this context, the extraordinary clinical benefits of BTZ treatment have to date been attributed to the exquisite intrinsic dependency of multiple myeloma cells on proteasome activity (17). Here, we challenge this notion by characterizing BTZ as an immunotherapeutic agent and delineating novel mechanisms whereby BTZ triggers a specific anti–multiple myeloma immune response.

The first major conclusion of our study is that BTZ efficacy is due to the activation of the immune system: Although the drug can efficiently delay tumor growth in immunodeficient mice, it requires a competent immune system to induce tumor regression. To explain this effect, we focused on a tumor-intrinsic mechanism of immune activation, specifically the induction of ICD. Although early *in vitro* studies have suggested an immunogenic role of BTZ (20), its biological, functional, and clinical significance is not fully characterized (23). In our studies, BTZ treatment led to the exposure of the eat-me molecule CALR on the cell surface of both human and murine multiple myeloma cell lines, and we confirmed the obligate role of this DAMP as a major prophagocytic checkpoint in multiple myeloma both *in vitro* and *in vivo*. Analysis of transcriptomic changes in murine multiple myeloma cells after BTZ treatment identified an ICD signature. Most importantly, we confirmed its clinical significance, because the analogous ICD signature was positively correlated with improved outcome of patients with multiple myeloma treated with BTZ in two independent datasets. Multiple clinical trials have shown that treatment with BTZ is effective in reducing tumor burden in patients with multiple myeloma, including multiple myeloma with high-risk cytogenetics such as t(4;14) (40). Based on these data, we speculated that clinical responses to BTZ may be mediated via the induction of an efficient anti–multiple myeloma immune response. Further characterization of the genes included in the BTZ-induced ICD signature identified a multiple myeloma cell–autonomous type I IFN response. This finding is consistent with a previous report showing that activation of a viral mimicry state in multiple myeloma cells increases the anti–multiple myeloma immune response to therapy in the murine Vk*MYC model of multiple myeloma (41). Moreover, IFNα has in the past been used, either alone or in combination, to treat patients with multiple myeloma; although it demonstrated efficacy, its clinical utility was limited by toxicity (42).

The second major conclusion of our study is that BTZ stimulates the immunogenicity of multiple myeloma cells by activating the cGAS/STING innate immune response signaling pathway (32, 35). The release of cytosolic DNA after BTZ-induced multiple myeloma cell death is a trigger for the STING pathway; an increased genomic instability, due to inhibition of the DNA repair machinery, is also recognized as a downstream effect of proteasome inhibition (18). Here, we showed that the expression of STING positively correlates with the expression of ICD-related ISGs in patients with multiple myeloma, implicating this pathway in BTZ-induced IFN response. Loss of IFN response has been described as an additional mechanism of tumor immune escape (43), and we found that patients with multiple myeloma with low STING/ISG expression do not efficiently respond to ICD induction after BTZ treatment. Indeed, immune response after BTZ treatment was significantly reduced *in vivo* against multiple myeloma tumors lacking *STING*. Importantly, activation of the STING pathway is an emerging immunotherapeutic approach, and phase I and II clinical trials of several STING agonists are currently ongoing in solid tumors or lymphoma, alone or in combination with immunotherapies (NCT04144140, NCT03937141, NCT02675439, NCT03172936, and NCT03010176). The prior use of IFN stimulation in anti–multiple myeloma therapy coupled with our current data suggests that STING agonists may also represent a promising therapeutic strategy in multiple myeloma and that their combined use with BTZ may increase their immunogenic effect, especially in patients with low basal level of STING expression. Indeed, we showed that combination of BTZ with the STING agonist ADU-S100 significantly enhanced the immunogenic effect of BTZ *in vivo*. These studies both validate STING as a therapeutic target and provide the framework for clinical trials evaluating BTZ and STING agonist combination therapy in multiple myeloma.

In summary, our study delineates the mechanism whereby BTZ induces a clinically significant antitumor immune response in multiple myeloma. Although BTZ is incorporated into many combination therapeutic regimens for multiple myeloma due to its direct impact on tumor cells, recognition of its immune effect will inform its broader use, alone and in combination, as an immunotherapy. In addition, induction of ICD may account for the enhanced clinical activity observed in patients with multiple myeloma currently treated with effective combinations incorporating BTZ with either IMiDs or mAbs. Finally, our study identifies and validates STING as a new therapeutic target mediating immune activation against multiple myeloma and provides the preclinical framework for STING agonist and BTZ combination clinical trials to enhance anti–multiple myeloma immune responses and further improve patient outcome in multiple myeloma.

METHODS

Cell Culture

Multiple myeloma cell lines U266, NCI-H929, murine JAWSII, and 293T were purchased from the American Type Culture Collection; AMO1 was purchased from DSMZ; and murine 5TGM1 cells were kindly provided by Dr. Irene Ghobrial [Dana-Farber Cancer Institute (DFCI), Boston, MA]. Cell lines were tested to rule out *Mycoplasma* contamination using the MycoAlert Mycoplasma Detection Kit (Lonza) and authenticated by short-tandem repeat DNA typing. Human multiple myeloma cell lines were cultured in RPMI/1640 media containing 10% FBS (GIBCO; Thermo Fisher Scientific), 2 μmol/L glutamine, 100 U/mL penicillin, and 100 μg/mL streptomycin (GIBCO; Thermo Fisher Scientific). 293T

cells were maintained in DMEM culture media with 10% FBS and 1% penicillin–streptomycin. Murine JAWSII cells were cultured in Alpha minimum essential medium with ribonucleosides, deoxyribonucleosides, 4 mmol/L L-glutamine, 1 mmol/L sodium pyruvate, 20% FBS, 1% penicillin–streptomycin, and 5 ng/mL murine GMCSF (PeproTech). Murine 5TGM1 cells were maintained in Iscove's modified Dulbecco's Media (Thermo Fisher Scientific) supplemented with 10% FBS and 1% penicillin–streptomycin.

Patient Multiple Myeloma Cells and Normal Donor Samples

Multiple myeloma patient BM aspirates and normal donor peripheral blood mononuclear cells (PBMC) were obtained after written informed consent in accordance with the Declaration of Helsinki and under the approval by the Institutional Review Board of the DFCI. BMMCs and PBMCs were separated by Ficoll-Paque PLUS (GE Healthcare). Multiple myeloma cells from BMMCs were enriched by CD138-positive selection using magnetic microbeads (Miltenyi Biotec).

Drugs and Reagents

BTZ was purchased from Selleckchem (S1013) and resuspended in DMSO. Anti-mouse IFNAR1 (Clone: MAR1-5A3; #BE0241) mAb and mouse IgG1 Isotype CNT mAb were purchased from BioXCell and resuspended in InVivoPure Dilution Buffer following the manufacturer's instructions. ADU-S100 (#CT-ADUS100) was purchased from ChemieTek.

Proliferation Assay

Cell viability was evaluated by Cell Counting Kit-8 (CCK-8) assay (Dojindo Molecular Technologies).

Apoptosis Assay

Apoptosis was evaluated by Annexin-V/7-Aminoactinomycin D (7-AAD) staining and flow cytometric analysis using the PE Annexin-V Apoptosis Detection Kit I (BD Biosciences).

Cell-Surface Exposure of CALR

Multiple myeloma cells were seeded in 12-well plates (2×10^5 per well), treated with BTZ for 16 hours at indicated concentrations, and then stained with Alexa Fluor647 anti-CALR antibody (ab196159, Abcam) and 7-AAD. Analysis of fluorescence intensity on 7-AAD–negative cells was done using BD LRSFortessa X-20 flow cytometer.

Generation of Mo-DCs and Phagocytosis Assay

Mo-DCs were generated from $CD14^+$ peripheral blood monocytes from healthy donors, positively selected using magnetic beads (Miltenyi Biotec), cultured for 6 days in Mo-DC differentiation medium containing GMCSF and IL4 (130-094-812; Miltenyi Biotec). AMO1 and NCI-H929 cells lines, as well as patient multiple myeloma cells, were stained with CellTrace Far Red (Thermo Fisher Scientific), cultured with or without BTZ for 16 hours, and then incubated in 48-well plates for 4 hours at 1:1 ratio with CellTrace CFSE-stained Mo-DCs. Cells were then collected, and phagocytosis analysis was performed by flow cytometry and confocal microscopy. Analogous phagocytosis experiments were performed using 5TGM1 murine multiple myeloma and JAWSII cell lines that were used as source of immature murine DCs.

Flow Cytometry–Based Assay

Collected cells were analyzed using the BD LRSFortessa X-20 flow cytometer. Mo-DCs that engulfed multiple myeloma cells were CFSE and Far Red double positive. Fold increase in percentage of double-positive DCs after coculture with BTZ-treated versus untreated multiple myeloma cells was compared.

Confocal Microscopy–Based Assay

5TGM1 cells (15,000) were cytospun for 7 minutes at 300 rpm, fixed in 4% paraformaldehyde for 20 minutes at room temperature, and washed three times with 1% FBS in PBS. After washes, nuclear content was stained with Fluoro-gel II mounting medium with DAPI (Thermo Fisher Scientific). Slides were examined using Yokogawa Spinning Disk Confocal/TIRF System and analyzed with ImageJ software.

DC Maturation Assay

Immature DCs were generated as described above ("Generation of Mo-DCs and Phagocytosis Assay" section). DCs were cultured alone or with untreated or BTZ-pretreated AMO1 (5 nmol/L) for 24 hours. DCs alone were cultured (i) without maturation stimuli, (ii) with 50 ng/mL of TNFα (Millipore Sigma), or (iii) with 5 nmol/L of BTZ. After 24 hours, cells were harvested and analyzed by flow cytometry using the following Abs: anti–CD83-APC (#551073), CD86-FITC (#555657), and 7-AAD from BD Biosciences and CD11c-BV650 from BioLegend (#563404). Dead cells were excluded by 7-AAD positivity, and CD83 and CD86 expression was evaluated on $CD11c^+$ cells.

Generation of CRISPR KO Multiple Myeloma Cells

Single-guide RNA (sgRNA) targeting murine *Calr*, murine *Sting/Tmem173*, and human *STING/TMEM173* were used to generate 5TGM1 $Calr^{KO}$, 5TGM1 $STING^{KO}$, and AMO1 $STING^{KO}$ cells. All cell lines were transfected via electroporation (Neon Transfection System; Thermo Fisher Scientific) using All-in-one vectors (pCLIP-ALL-hCMV-ZsGreen) containing an sgRNA and a Cas9 (transOMIC technologies). Forty-eight hours after electroporation, cells were ZsGreen-sorted and plated as monoclones in 96-well plates. After expansion, monoclones were screened for either CALR or STING expression by Western blot (WB). The following sgRNA sequences were used:

Calr Mus Musculus:
- sgRNA#1:TATGTTTGGATTCGACCCAG
- sgRNA#2:ATAGATGGCAGGGTCTGCGG
- sgRNA#3:CGTAAAATTTGCCAGAACTG
- Non targeting control: GGAGCGCACCATCTTCTTCA

Sting/Tmem173 Mus Musculus:
- sgRNA#1:TATCTCGGAATCGAATGTTG
- sgRNA#2:GAAGGCCAAACATCCAACTG
- sgRNA#3:CTACATAACAACATGCTCAG

STING/TMEM173 Homo Sapiens:
- sgRNA#1:ACAGCAGCAACAGGGCCCCA
- sgRNA#2:ATAGATGGACAGCAGCAACA
- sgRNA#3:GCAGCAACAGGGCCCCACGG

Stable Overexpression of CALR in 5TGM1 $Calr^{KO}$ Clones

The pRetroX-CRT-GPI-IRES-DsRed plasmid containing full-length murine CALR cDNA was kindly provided by Chen and colleagues (44). Virus was generated by transfecting HEK293T cells with 4 μg of DNA and packaging vectors (4 μg of psPAX2 and 2 μg of pMD2.G) using lipofectamine 2000 (Thermo Fisher Scientific). Supernatant containing viral particles was harvested after 48 hours and sterile 0.45 μm filtered. 5TGM1 $Calr^{KO}$ clones were spinoculated for 1 hour with media containing lentiviral particles at a multiplicity of infection of 2 in the presence of 8 μg/mL polybrene. Media were then changed, and cells were DsRed-sorted using M Aria II SORP UV (BD Biosciences). After sorting, efficient overexpression was evaluated by WB.

Immunoblotting

Cell lysis was performed in RIPA buffer (Boston Bio Products) supplemented with Halt protease and phosphatase inhibitor cocktail (Thermo Fisher Scientific). SDS-PAGE was performed on NuPage Bis-Tris gels (Thermo Fisher Scientific) using MOPS or MES running

buffer. Gels were dry transferred onto 0.45 μm nitrocellulose membranes using the iBlot Dry Blotting System (Thermo Fisher Scientific).

The following Abs were purchased from Cell Signaling Technology: EIF2A (#5324), p-EIF2A (#3398), ATF4 (#11815), CHOP (2895), CALR (#12238), cGAS (#15102), TBK1 (#3504), pTBK1 (#5483), pIRF3 (#29047), and STING (#13647). GAPDH (#2118) and B-ACTIN (#4970) were used as loading controls.

Reverse Transcription and Quantitative Real-Time PCR

Total RNA from multiple myeloma cells was prepared with TRIzol (Thermo Fisher Scientific) and RNA Clean and Concentrator-5 kit (Zymo Research) following the product instructions. RNA integrity and quantity were assessed by NanoDrop Spectrophotometer (Thermo Fisher Scientific). For analysis of mRNA expression, oligo-dT–primed cDNA was obtained using the High-Capacity cDNA Reverse Transcription Kit (Thermo Fisher Scientific) and used as template to quantify human and murine *IFNA1* (Hs03044218_g1, Mm03030145_gH), human and murine *IFNB1* (Hs01077958_s1, Mm00439552_s1), human and murine *CXCL9* (Hs00171065_m1, Mm00434946_m1), and human and murine *GAPDH* (Hs02786624_g1, Mm99999915_g1). Analysis was determined by RT-PCR using TaqManFast Universal PCR Master Mix on a 7500 Fast Real-Time PCR System (Thermo Fisher Scientific). Comparative RT-PCR was performed in triplicate. Relative expression was calculated using the comparative cross threshold (Ct) method.

Analysis of T-cell Priming

DCs were generated from PBMCs of healthy donors as described above ("Generation of Mo-DCs and Phagocytosis Assay" section). T cells were negatively selected from $CD14^-$ PBMCs from the same donors using the Pan T Cell Isolation Kit (Miltenyi Biotec) and frozen until immature DCs were generated. Either untreated or BTZ-treated multiple myeloma cells were cocultured with DCs and T cells for 5 days. T cells and DCs were similarly cultured in the absence of multiple myeloma cells and in the presence of BTZ. Before analysis, cells were treated with Dynabeads Human T-Activator CD3/CD28 (#11131D, Thermo Fisher Scientific), and with GolgiStop and GolgiPlug (#554724 and #555029, BD Biosciences). T-cell populations were analyzed using 10-color flow cytometry with the following Abs: CD3-BV605 (#317322), CD8-FITC (#344704), CD4-PerCP/Cyanine5.5 (#317428), CD45RO-APC (#304210), CCR7-PE (#353204), CD69-PE/Cyanine7 (#310912), IL2-BV785 (#500348), IFNγ-BV421 (#502532; BioLegend), and PD1-Super Bright 702 (#67-998-582). LIVE/DEAD Fixable Aqua dead Cell Stain (#L34966; Thermo Fisher Scientific) was also added to discriminate dead cells. Intracellular staining for IL2 and IFNγ was performed using the Fixation/Permeabilization Solution Kit (BD Biosciences).

When T-cell experiments were performed using patient multiple myeloma cells, the entire population of autologous BMMCs was cultured in the presence and absence of BTZ and analyzed after 5 days. Data from experiments performed using multiple myeloma cell lines were analyzed with a bioinformatic semiautomated pipeline (45). Briefly, flow cytometry files were entered in a custom R script that includes different bioinformatic algorithms and has been designed to reduce the impact of technical and instrumental differences, minimize the variability of manual analysis, and reveal full cellular diversity based on automatic semisupervised clustering. Data from primary patients with multiple myeloma were manually analyzed by using Infinicyt 2.0 (Cytognos).

Analysis of Naïve T-cell Proliferation

DCs were generated from PBMCs of healthy donors as described above ("Generation of Mo-DCs and Phagocytosis Assay" section). Naïve T cells were negatively selected from $CD14^-$ PBMCs from the same donors using the Naive Pan T Cell Isolation Kit (Miltenyi Biotec) and frozen. When DCs were generated, either untreated or BTZ-treated multiple myeloma cells were cocultured with DCs and naïve T cells labeled with CellTrace Violet Cell Proliferation Kit (Thermo Fisher Scientific) for 5 days. Naïve T cells were also cultured in the absence of multiple myeloma cells and in the presence of phytohemagglutinin (20 μg/mL) as positive control. Before analysis, cells were stained with CD8-FITC (#344704), CD4-PerCP/Cyanine5.5 (#317428; BioLegend), and LIVE/DEAD Fixable Aqua dead Cell Stain (#L34966; Thermo Fisher Scientific). Proliferating CD4 and CD8 T-cell subsets were then analyzed using the FlowJo software (Becton, Dickinson & Company).

Cytotoxicity Assay

After coculture of HLA-matched DCs and T cells from healthy donors with either untreated or BTZ-treated U266 cells for 5 days, T cells were negatively selected using the Pan T cell Isolation Kit (Miltenyi Biotec) and plated in round-bottom 96-well plates with naïve U266 cells prestained with CFSE dye (Thermo Fisher Scientific) at different target:effector ratios for 24 hours in the presence of IL2 (#130-097-74, Miltenyi Biotec). Then cells were 7-AAD stained, and detection of viable CFSE-gated cells was performed using BD LRSFortessa X-20 cytometer.

Micronuclei Assay

Cells were analyzed for micronuclei formation using a flow cytometry–based Micronucleus Assay (MicroFlow kit), according to the manufacturer's protocol. Briefly, nonviable cells were removed by Ficoll gradient centrifugation. Viable cells were then stained with photo-activated Nucleic Acid Dye A (ethidium monoazide) that crosses the compromised outer membrane of apoptotic and necrotic cells and stains them red. Cells were then washed twice and lysed with a detergent containing buffer to break open cytoplasmic membranes and release nuclei and micronuclei. Nucleic Acid Dye B (SYTOX green) was then added to label DNA from both nuclei and micronuclei. Flow cytometry analysis was used to distinguish DNA from dead (dual stained with Dyes A and B) and live (single stained with Dye B) cells. After removing dead cells from the analysis, micronuclei were quantified and plotted as a percentage of 2N nuclei based on Dye B (SYTOX green) staining intensity and exhibited 1/100th to 1/10th the fluorescent intensity of 2N nuclei.

ELISA

$AMO1^{WT}$ and $STING^{KO}$ cells were either untreated or treated with BTZ for 24 hours. Supernatant was collected, and secretion of CXCL9 chemokines was analyzed by MIG (CXCL9) Human Instant ELISA Kit (#BMS285INST, Thermo Fisher Scientific).

In Vivo *Studies*

Six-week-old female immunodeficient NOD.CB17-Prkdcscid/NCrCrl (NOD/SCID; Charles River) and immunocompetent C57BL/KaLwRijHsd (Envigo) mice were housed in our animal facility at DFCI. All experiments were performed after approval by the Animal Ethics Committee of the DFCI and performed using institutional guidelines.

In Vivo *Studies for Tumor Growth Analysis*

NOD/SCID and C57BL/KaLwRijHsd mice were s.c. injected with 1×10^6 5TGM1 either WT or $Calr^{KO}$ cells in PBS. When tumors became measurable, mice were randomized to receive either PBS or BTZ administered i.p. 0.5 mg/kg twice/week for 2 weeks. Tumor sizes were measured as previously described (46), and mice were sacrificed when tumors reached 2 cm in diameter or ulceration or major compromise in quality of life. A parallel experiment was performed to allow for tumor harvesting after two injections intraperitoneally of BTZ for RNA-seq analysis, as detailed below.

For BTZ and STING agonist combination studies, C57BL/KaLwRijHsd (n = 5/group) and SCID/NOD (n = 6/group) mice bearing $5TGM1^{WT}$ and C57BL/KaLwRijHsd mice (n = 5/group) bearing 5TGM1 $STING^{KO}$ tumors were randomized to receive PBS, BTZ

(0.375 mg/kg twice a week for 2 weeks, i.p.), ADU-S100 (100 μg) administered in the peritumoral area (days 1 and 2), or a combination. Tumor sizes were measured as described above. A parallel experiment in C57BL/KaLwRijHsd mice was performed to allow for tumor harvesting after one administration of either BTZ or ADU-S100. Tumors were fixed in 10% formalin for 24 hours and then maintained in 70% ethanol prior to paraffin embedding and processing for IHC to detect CD3 (#nb600 Ab, Novus Bio).

In Vivo *Rechallenge of Viable 5TGM1 Cells in BTZ-Treated Mice*

C57BL/KaLwRijHsd mice bearing 5TGM1^{WT} tumors were treated with BTZ as above. Two weeks after observation of tumor regression, treated ($n = 5$) as well as naïve mice ($n = 5$) were rechallenged with viable 1×10^6 5TGM1^{WT} cells, and tumor growth was monitored over time. In a parallel experiment, spleens were harvested 2 weeks after tumor rechallenge from both groups to test T-cell–specific reactivity against multiple myeloma cells by ELISPOT assay (Translational Immunogenomics Laboratory, DFCI).

Vaccination Studies

5×10^5 5TGM1^{WT} or *Calr*^{KO} cells were treated with BTZ (7.5 nmol/L) *in vitro* for 16 hours. C57BL/KaLwRijHsd mice ($n = 8$/group) were then either vaccinated subcutaneously with dying 5TGM1^{WT} or 5TGM1*Calr*^{KO} cells or not vaccinated. After 1 week, viable 1×10^6 WT 5TGM1 cells were injected s.c., and tumor growth was monitored over time.

RNA-seq Analysis from Mouse Tumors

Tumors growing from both 5TGM1^{WT} or *Calr*^{KO} cells in C57BL/KaLwRijHsd mice treated with either PBS or BTZ (three/group) were harvested and used to extract RNA using the RNeasy kit (QIAGEN). After passing quality control, RNA-seq was performed using Illumina NextSeq 500 Single-End 75 bp (SE75) and analyzed following the VIPER (Visualization Pipeline for RNA-seq) next-generation sequencing (NGS) analysis pipeline (47), comparing BTZ-treated mice versus PBS in each experimental setting. Lists of differentially expressed genes (DEG) were applied to gene set enrichment analysis (GSEA) and Cytoscape (48, 49) software to reveal biological pathways modulated by BTZ. Focused analysis was conducted on the list of DEGs included in the gene sets of the Hallmarks collection of the Molecular Signature Database conveying immune processes and enriched in 5TGM1^{WT} tumors after treatment with BTZ. Analysis of expression of human orthologs of these 90 genes in patients with multiple myeloma and correlation with patient clinical outcome was then analyzed as detailed below. RNA-seq data have been submitted to Gene Expression Omnibus (GEO; accession number: GSE171837).

RNA-seq Analysis of AMO1 Multiple Myeloma Cells after Treatment with BTZ

AMO1 WT and *STING*^{KO} were cultured for 16 hours in the presence or absence of BTZ (5 nmol/L). RNA was extracted as previously described and submitted to NovaSeq RNA-seq analysis followed by VIPER NGS analysis (47). Lists of DEGs were applied to the GSEA software. RNA-seq data have been submitted to GEO (accession number: GSE171837).

Analysis of RNA-seq Data of Patients with Multiple Myeloma

We used RNA-seq from CD138$^+$ multiple myeloma cells from a previously published dataset of 327 newly diagnosed clinically annotated patients with multiple myeloma from the IFM/DFCI 2009 clinical trial (NCT01191060; ref. 50). After quality control, all RNA-seq data were quantified with Salmon. Raw counts and transcripts per million values were summed to gene levels using tximport, and DESeq2 was used for all differential gene expression analysis. Centered and scaled data were used for clustering with ward.D2 algorithm. All figures were created with pheatmap or ggplot2. Survival analysis was performed using survival package in R, and the log-rank test was used to compare groups. As validation dataset, gene expression data of 152 patients with multiple myeloma performed with microarray platform were downloaded from GEO (GSE9782; ref. 26) and preprocessed and normalized with affy and limma packages in R.

Statistical Analysis

All *in vitro* experiments were repeated at least three times and performed in triplicate. Statistical significance of differences was determined using the Student *t* test (unless otherwise specified). All statistical analyses and graphs were performed using GraphPad software.

Authors' Disclosures

A. Gulla reports grants from Leukemia & Lymphoma Society, American Society of Hematology, and NIH/NCI during the conduct of the study, as well as a patent for Modulating Gabarap to Modulate Immunogenic Cell Death pending. G. Bianchi reports grants from American Society of Hematology, International Myeloma Foundation, and Damon Runyon Cancer Research Foundation and personal fees from Pfizer, Karyopharm, and MJH outside the submitted work. P.G. Richardson reports grants and personal fees from Oncopeptides, Celgene/Bristol Myers Squibb, and Takeda and personal fees from Janssen, Sanofi, Secura Bio, GlaxoSmithKline, and Regeneron during the conduct of the study. D. Chauhan reports other support from Stemline Therapeutics, Oncopeptides, and C4 Therapeutics outside the submitted work. N.C. Munshi reports personal fees from Takeda, Bristol Myers Squibb, OncoPep, Janssen, Amgen, AbbVie, Adaptive Biotechnology, Karyopharm, and Legend Biotech during the conduct of the study, as well as a patent for OncoPep issued. K.C. Anderson reports personal fees from Amgen and Millennium/Takeda during the conduct of the study, as well as personal fees from Pfizer, AstraZeneca, Janssen, Precision Biosciences, Mana, Windmill, Starton, Raqia, C4 Therapeutics, and OncoPep outside the submitted work. No disclosures were reported by the other authors.

One of the Editors-in-Chief is an author on this article. In keeping with the AACR's editorial policy, the peer review of this submission was managed by a member of *Blood Cancer Discovery*'s Board of Scientific Editors, who rendered the final decision concerning acceptability.

Authors' Contributions

A. Gulla: Conceptualization, resources, data curation, formal analysis, supervision, funding acquisition, validation, investigation, visualization, methodology, writing–original draft. **E. Morelli:** Validation, investigation, methodology, writing–review and editing. **M.K. Samur:** Resources, software, formal analysis, writing–review and editing. **C. Botta:** Investigation. **T. Hideshima:** Investigation, writing–review and editing. **G. Bianchi:** Resources. **M. Fulciniti:** Investigation. **S. Malvestiti:** Investigation. **R.H. Prabhala:** Investigation. **S. Talluri:** Investigation. **K. Wen:** Investigation. **Y.-Z. Tai:** Resources. **P.G. Richardson:** Resources. **D. Chauhan:** Writing–review and editing. **T. Sewastianik:** Investigation. **R.D. Carrasco:** Investigation. **N.C. Munshi:** Resources, supervision. **K.C. Anderson:** Conceptualization, resources, supervision, funding acquisition, writing–original draft, writing–review and editing.

Acknowledgments

The authors thank Derin Keskin and the Translational Immunogenomics Lab at Dana-Farber Cancer Institute for the scientific advice and technical support to perform the ELISPOT assay for immune monitoring *in vivo*. E. Morelli is a recipient of the Brian D.

Novis Junior Grant (2021/2022) from the International Myeloma Foundation.

This work is supported by NIH/NCI grants SPORE-P50CA100707 (K.C. Anderson and N.C. Munshi), R01-CA050947 (K.C. Anderson), R01CA207237 (K.C. Anderson and D. Chauhan), P01CA155258 (K.C. Anderson and N.C. Munshi), and R01-CA178264 (K.C. Anderson and T. Hideshima); VA Healthcare System grant number 5I01BX001584 (N.C. Munshi); the Dr. Miriam and Sheldon G. Adelson Medical Research Foundation (K.C. Anderson); and a Paula and Rodger Riney Foundation grant (K.C. Anderson). A. Gulla is a Fellow of the Leukemia & Lymphoma Society and a Scholar of the American Society of Hematology.

Received March 12, 2021; revised March 15, 2021; accepted April 16, 2021; published first April 23, 2021.

REFERENCES

1. Gulla A, Anderson KC. Multiple myeloma: the (r)evolution of current therapy and a glance into future. Haematologica 2020;105:2358–67.
2. Kumar SK, Rajkumar V, Kyle RA, van Duin M, Sonneveld P, Mateos MV, et al. Multiple myeloma. Nat Rev Dis Primers 2017;3:17046.
3. Nakamura K, Smyth MJ, Martinet L. Cancer immunoediting and immune dysregulation in multiple myeloma. Blood 2020;136:2731–40.
4. Wudhikarn K, Wills B, Lesokhin AM. Monoclonal antibodies in multiple myeloma: current and emerging targets and mechanisms of action. Best Pract Res Clin Haematol 2020;33:101143.
5. Galluzzi L, Buque A, Kepp O, Zitvogel L, Kroemer G. Immunological effects of conventional chemotherapy and targeted anticancer agents. Cancer Cell 2015;28:690–714.
6. Kroemer G, Galluzzi L, Kepp O, Zitvogel L. Immunogenic cell death in cancer therapy. Annu Rev Immunol 2013;31:51–72.
7. Casares N, Pequignot MO, Tesniere A, Ghiringhelli F, Roux S, Chaput N, et al. Caspase-dependent immunogenicity of doxorubicin-induced tumor cell death. J Exp Med 2005;202:1691–701.
8. Galluzzi L, Vitale I, Warren S, Adjemian S, Agostinis P, Martinez AB, et al. Consensus guidelines for the definition, detection and interpretation of immunogenic cell death. J Immunother Cancer 2020;8:e000337.
9. Bloy N, Garcia P, Laumont CM, Pitt JM, Sistigu A, Stoll G, et al. Immunogenic stress and death of cancer cells: contribution of antigenicity vs adjuvanticity to immunosurveillance. Immunol Rev 2017;280:165–74.
10. Obeid M, Tesniere A, Ghiringhelli F, Fimia GM, Apetoh L, Perfettini JL, et al. Calreticulin exposure dictates the immunogenicity of cancer cell death. Nat Med 2007;13:54–61.
11. Zitvogel L, Apetoh L, Ghiringhelli F, Andre F, Tesniere A, Kroemer G. The anticancer immune response: indispensable for therapeutic success? J Clin Invest 2008;118:1991–2001.
12. Galluzzi L, Humeau J, Buque A, Zitvogel L, Kroemer G. Immunostimulation with chemotherapy in the era of immune checkpoint inhibitors. Nat Rev Clin Oncol 2020;17:725–41.
13. Kepp O, Zitvogel L, Kroemer G. Clinical evidence that immunogenic cell death sensitizes to PD-1/PD-L1 blockade. Oncoimmunology 2019;8:e1637188.
14. Richardson PG, Sonneveld P, Schuster M, Irwin D, Stadtmauer E, Facon T, et al. Extended follow-up of a phase 3 trial in relapsed multiple myeloma: final time-to-event results of the APEX trial. Blood 2007;110:3557–60.
15. Richardson PG, Sonneveld P, Schuster MW, Irwin D, Stadtmauer EA, Facon T, et al. Bortezomib or high-dose dexamethasone for relapsed multiple myeloma. N Engl J Med 2005;352:2487–98.
16. Bianchi G, Oliva L, Cascio P, Pengo N, Fontana F, Cerruti F, et al. The proteasome load versus capacity balance determines apoptotic sensitivity of multiple myeloma cells to proteasome inhibition. Blood 2009;113:3040–9.
17. Gandolfi S, Laubach JP, Hideshima T, Chauhan D, Anderson KC, Richardson PG. The proteasome and proteasome inhibitors in multiple myeloma. Cancer Metastasis Rev 2017;36:561–84.
18. Neri P, Ren L, Gratton K, Stebner E, Johnson J, Klimowicz A, et al. Bortezomib-induced "BRCAness" sensitizes multiple myeloma cells to PARP inhibitors. Blood 2011;118:6368–79.
19. Accardi F, Toscani D, Bolzoni M, Dalla Palma B, Aversa F, Giuliani N. Mechanism of action of bortezomib and the new proteasome inhibitors on myeloma cells and the bone microenvironment: impact on myeloma-induced alterations of bone remodeling. Biomed Res Int 2015;2015:172458.
20. Spisek R, Charalambous A, Mazumder A, Vesole DH, Jagannath S, Dhodapkar MV. Bortezomib enhances dendritic cell (DC)-mediated induction of immunity to human myeloma via exposure of cell surface heat shock protein 90 on dying tumor cells: therapeutic implications. Blood 2007;109:4839–45.
21. Serrano-Del Valle A, Anel A, Naval J, Marzo I. Immunogenic cell death and immunotherapy of multiple myeloma. Front Cell Dev Biol 2019;7:50.
22. Jarauta V, Jaime P, Gonzalo O, de Miguel D, Ramirez-Labrada A, Martinez-Lostao L, et al. Inhibition of autophagy with chloroquine potentiates carfilzomib-induced apoptosis in myeloma cells in vitro and in vivo. Cancer Lett 2016;382:1–10.
23. De Beck L, Melhaoui S, De Veirman K, Menu E, De Bruyne E, Vanderkerken K, et al. Epigenetic treatment of multiple myeloma mediates tumor intrinsic and extrinsic immunomodulatory effects. Oncoimmunology 2018;7:e1484981.
24. Maes K, Boeckx B, Vlummens P, De Veirman K, Menu E, Vanderkerken K, et al. The genetic landscape of 5T models for multiple myeloma. Sci Rep 2018;8:15030.
25. Attal M, Lauwers-Cances V, Hulin C, Leleu X, Caillot D, Escoffre M, et al. Lenalidomide, bortezomib, and dexamethasone with transplantation for myeloma. N Engl J Med 2017;376:1311–20.
26. Mulligan G, Mitsiades C, Bryant B, Zhan F, Chng WJ, Roels S, et al. Gene expression profiling and correlation with outcome in clinical trials of the proteasome inhibitor bortezomib. Blood 2007;109:3177–88.
27. Rusinova I, Forster S, Yu S, Kannan A, Masse M, Cumming H, et al. Interferome v2.0: an updated database of annotated interferon-regulated genes. Nucleic Acids Res 2013;41:D1040–6.
28. Vacchelli E, Sistigu A, Yamazaki T, Vitale I, Zitvogel L, Kroemer G. Autocrine signaling of type 1 interferons in successful anticancer chemotherapy. Oncoimmunology 2015;4:e988042.
29. Sistigu A, Yamazaki T, Vacchelli E, Chaba K, Enot DP, Adam J, et al. Cancer cell-autonomous contribution of type I interferon signaling to the efficacy of chemotherapy. Nat Med 2014;20:1301–9.
30. Zitvogel L, Galluzzi L, Kepp O, Smyth MJ, Kroemer G. Type I interferons in anticancer immunity. Nat Rev Immunol 2015;15:405–14.
31. Zhang CZ, Spektor A, Cornils H, Francis JM, Jackson EK, Liu S, et al. Chromothripsis from DNA damage in micronuclei. Nature 2015;522:179–84.
32. Mackenzie KJ, Carroll P, Martin CA, Murina O, Fluteau A, Simpson DJ, et al. cGAS surveillance of micronuclei links genome instability to innate immunity. Nature 2017;548:461–5.
33. Motwani M, Fitzgerald KA. cGAS Micro-manages genotoxic stress. Immunity 2017;47:616–7.
34. Reislander T, Groelly FJ, Tarsounas M. DNA damage and cancer immunotherapy: a STING in the tale. Mol Cell 2020;80:21–8.
35. Hopfner KP, Hornung V. Molecular mechanisms and cellular functions of cGAS-STING signalling. Nat Rev Mol Cell Biol 2020;21:501–21.
36. Flood BA, Higgs EF, Li S, Luke JJ, Gajewski TF. STING pathway agonism as a cancer therapeutic. Immunol Rev 2019;290:24–38.
37. Corrales L, McWhirter SM, Dubensky TW Jr, Gajewski TF. The host STING pathway at the interface of cancer and immunity. J Clin Invest 2016;126:2404–11.
38. Sivick KE, Desbien AL, Glickman LH, Reiner GL, Corrales L, Surh NH, et al. Magnitude of therapeutic STING activation determines CD8(+) T cell-mediated anti-tumor immunity. Cell Rep 2019;29:785–9.
39. Corrales L, Glickman LH, McWhirter SM, Kanne DB, Sivick KE, Katibah GE, et al. Direct activation of STING in the tumor microenvironment leads to potent and systemic tumor regression and immunity. Cell Rep 2015;11:1018–30.

40. Avet-Loiseau H, Leleu X, Roussel M, Moreau P, Guerin-Charbonnel C, Caillot D, et al. Bortezomib plus dexamethasone induction improves outcome of patients with t(4;14) myeloma but not outcome of patients with del(17p). J Clin Oncol 2010;28:4630–4.
41. Chesi M, Mirza NN, Garbitt VM, Sharik ME, Dueck AC, Asmann YW, et al. IAP antagonists induce anti-tumor immunity in multiple myeloma. Nat Med 2016;22:1411–20.
42. Zhang L, Tai YT, Ho MZG, Qiu L, Anderson KC. Interferon-alpha-based immunotherapies in the treatment of B cell-derived hematologic neoplasms in today's treat-to-target era. Exp Hematol Oncol 2017;6:20.
43. Zaretsky JM, Garcia-Diaz A, Shin DS, Escuin-Ordinas H, Hugo W, Hu-Lieskovan S, et al. Mutations associated with acquired resistance to PD-1 blockade in melanoma. N Engl J Med 2016;375:819–29.
44. Chen X, Fosco D, Kline DE, Kline J. Calreticulin promotes immunity and type I interferon-dependent survival in mice with acute myeloid leukemia. Oncoimmunology 2017;6:e1278332.
45. Perez C, Botta C, Zabaleta A, Puig N, Cedena MT, Goicoechea I, et al. Immunogenomic identification and characterization of granulocytic myeloid-derived suppressor cells in multiple myeloma. Blood 2020;136:199–209.
46. Gulla A, Hideshima T, Bianchi G, Fulciniti M, Kemal Samur M, Qi J, et al. Protein arginine methyltransferase 5 has prognostic relevance and is a druggable target in multiple myeloma. Leukemia 2018;32:996–1002.
47. Cornwell M, Vangala M, Taing L, Herbert Z, Koster J, Li B, et al. VIPER: Visualization Pipeline for RNA-seq, a Snakemake workflow for efficient and complete RNA-seq analysis. BMC Bioinformatics 2018;19:135.
48. Bindea G, Mlecnik B, Hackl H, Charoentong P, Tosolini M, Kirilovsky A, et al. ClueGO: a Cytoscape plug-in to decipher functionally grouped gene ontology and pathway annotation networks. Bioinformatics 2009;25:1091–3.
49. Bindea G, Galon J, Mlecnik B. CluePedia Cytoscape plugin: pathway insights using integrated experimental and in silico data. Bioinformatics 2013;29:661–3.
50. Samur MK, Minvielle S, Gulla A, Fulciniti M, Cleynen A, Aktas Samur A, et al. Long intergenic non-coding RNAs have an independent impact on survival in multiple myeloma. Leukemia 2018;32:2626–35.